Renner-Teller effect on dissociative electron attachment to carbon dioxide

Bin Wu, Lei Xia, Yong-Feng Wang, Hong-Kai Li, Xian-Jin Zeng, and Shan Xi Tian*

Hefei National Laboratory for Physical Sciences at the Microscale and Department of Chemical Physics, University of Science and Technology of China, Hefei, Anhui 230026, China

(Received 30 October 2011; revised manuscript received 14 April 2012; published 17 May 2012)

Stereodynamics of dissociative electron attachment to CO_2 is investigated using O^- anion velocity imaging experiments. Here $^2\Pi_g$ as a Feshbach resonant state of CO_2^- is confirmed to play a role in the dissociation $CO_2^- \rightarrow CO(^1\Sigma^+) + O^-(^2P)$ around 8.0 eV. At the lower energy, 7.7 eV, two split states of $^2\Pi_g$ due to the Renner-Teller effect are found to couple with the dissociation path; while above this energy, at 8.2 and 8.7 eV, the coupling between the dissociation and the C-O bond stretching becomes predominant. The evolutions of the potential energy surface around this Feshbach resonant state result in the dramatically different angular distributions of the O^- momentum.

DOI: 10.1103/PhysRevA.85.052709 PACS number(s): 34.80.Ht, 34.80.Gs, 34.80.Bm

I. INTRODUCTION

The Renner-Teller (RT) effect originates from vibronic couplings between electron motions and nuclear vibrations in a linear triatomic molecule in the degenerate electronic state [1,2]. It has been investigated extensively, providing dynamics information of the potential energy surface (PES) of neutral or cationic species. The complex PES (CPES), $E_{\text{complex}}(R) = E_r(R) - i\Gamma(R)/2$, in which E_r is the energy position of an electron-molecule resonant state and Γ is the resonant energy width, is another type of PES controlling the formation of the resonant system and the subsequent decaying dynamics [3]. However, in the electron-molecule resonant system (also known as the temporary negative ion, TNI), very little is known about the dynamic coupling between nuclear and electron motions [4,5]. The RT effect as a typical vibronic coupling deserves to be investigated, especially in the complex PES of TNIs.

CO_2 represents a particularly interesting system for such study because this linear molecule ($D_{\infty h}$) at the electronic ground state may undergo structural bending when it captures a low-energy electron. It has been found that the vibration excitations of different modes are highly selective via the $^2\Pi_u$ shape resonance CO_2^- formed in low-energy electron attachments around 3.6 eV [5]. The nuclear motions leading to the RT effect were further analyzed theoretically on the basis of two asymptotic $^2A_1$ and $^2B_1$ states as the splitting components of the $^2\Pi_u$ resonance [6]. Electron autodetachment and the dissociations to anionic and neutral fragments are two main decaying channels of TNIs. Experimental studies of dissociative electron attachment (DEA) to CO_2 have been carried out by the different groups, primarily focusing on the yield efficiency and kinetic energy distributions of O^- [7–13]. The DEA path, $e^- + CO_2(^1\Sigma_g^+) \rightarrow CO_2^-(^2\Pi_u) \rightarrow CO(^1\Sigma^+) + O^-(^2P)$, can be accessed at low energies (4–5 eV) since its thermodynamic threshold lies at 3.99 eV. However, there are long-term arguments about the broad O^- yield peak at 7–9 eV [7–13]: Is it still related to the asymptotic components $^2A_1$ and $^2B_1$ of the lowest CO_2^- ($^2\Pi_u$) resonant state [6] or another shape resonant state, CO_2^- ($^2\Sigma_g^+$), proposed by Claydon *et al.* [14] and England *et al.* [15]? However, the latter was disputed, meanwhile a Feshbach resonant state $^2\Pi_g$ was proposed [12]. Two different dissociation channels with the common products [$CO(^1\Sigma^+) + O^-(^2P)$], namely, via $^2\Sigma_g^+$ at the lower energy and via $^2\Pi_g$ at the higher energy in the vertical electron attachments, were also postulated [16]. According to the kinetic energy distributions of O^- measured by Chantry [9] and Dressler and Allan [13], some anions of O^- have low kinetic energy (near 0 eV) while the others have energy of ca. 0.6 eV. The source of these O^- anions with the different kinetic energies is another debate of the past several decades. It was believed that such distinct dynamic behaviors should be strongly dependent on the topographic property of the CPES [17]. Herein, these puzzling misconceptions will be clarified. In the Franck-Condon region of the vertical electron attachment, we demonstrate the dynamic RT effect of the complex PES of CO_2^- on the O^- momentum distributions by the anion velocity image mapping experiments.

II. EXPERIMENTAL METHOD

Our newly developed anion velocity image mapping apparatus has been described in detail elsewhere [18]. In brief, an effusive molecular beam is perpendicular to the pulsed low-energy electron beam which is emitted from a homemade electron gun; these low-energy electrons are collimated with the homogenous magnetic field (15–20 Gauss) produced by a pair of Helmholtz coils (diameter, 800 mm). The anionic fragment yields of the DEA are periodically (500 Hz) pushed out from the reaction area and then fly through the time-of-flight (TOF) tube (installed along the molecular beam axis, the total length of which is 360 mm). Ten electrodes of the TOF mass spectrometer are in charge of the spatial ($2 \times 2 \times 2$ mm^3) and velocity ($\Delta v/v \leqslant 2.5\%$) focusing of the anions. The anionic fragments produced during one electron-beam pulse expand in the three-dimensional space and form a Newton sphere. Finally they can be detected with a pair of microchannel plates (MCPs) and a phosphor screen. The three-dimensional O^- momentum distributions are directly recorded with a CCD camera using the time-sliced imaging technique [18,19], namely, a detection time-gate is realized

*sxtian@ustc.edu.cn

 ©2012 American Physical Society

with a high-voltage pulse (60 ns in width) added on the rear MCP.

III. RESULTS AND DISCUSSION

As shown in Fig. 1(a), the O^- product efficiency curve has been recorded at electron incident energies of less than 10 eV. The spectral profile is exactly the same as measured previously [9]; thus only two representative points (red circles) obtained in this work are shown. Two bands with peaks at 4.4 and 8.2 eV should be attributed to the shape resonant state $^2\Pi_u$ and the Feshbach state $^2\Pi_g$, respectively [20]. Here, we record the central slice images of the O^- momentum distributions at four typical incident energies: 4.4, 7.7, 8.2, and 8.7 eV.

The O^- production at 4.4 eV has been explicitly interpreted with the process $CO_2^-(^2\Pi_u) \rightarrow CO(^1\Sigma^+) + O^-(^2P)$ [5–13]. Due to the too low kinetic energies of these O^- ions (90% less than 0.2 eV) [9], it is difficult to map the anisotropic momentum distribution of O^- ions, although the anisotropy was proposed in both the experimental [5] and theoretical studies [6]. The theoretical differential cross sections (DCSs) considering the vibration excitations of the bond-bending mode around 4 eV indeed show little preference at 135° with respect to that at 90° [5,6]. Such anisotropic character is somehow indicated by the ellipse sliced image in Fig. 1(b), implying that the RT effect should play an essential role in the DEA process at the CO_2^- ($^2\Pi_u$) resonant state. However, the DEA occurring at this low energy is unsuitable to giving us more insight into the RT effect. We focus on the DEA dynamics around the second peak in Fig. 1(a).

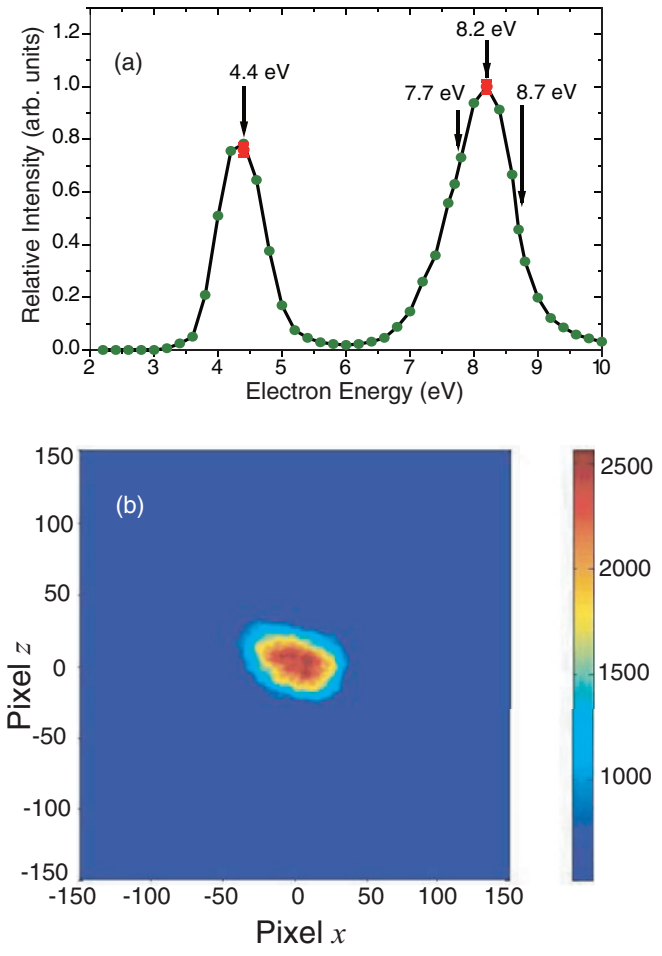

FIG. 1. (Color online) (a) The O^- production efficiency curves: the solid circles (green) are values adopted from the experimental work (at a temperature of 300 K) [9]; the solid circles with error bars (red) are values obtained in this work; and the arrows point to the incident energies at which the sliced images were recorded. (b) The sliced image of O^- recorded at an incident energy of 4.4 eV; the electron incident direction is from left to right.

To our surprise, three slice images recorded at 7.7, 8.2, and 8.7 eV, as shown in Figs. 2(a)–2(c), are distinctly different. A remarkable backward-scattering pattern is exhibited at 7.7 eV in Fig. 2(a), although there are another two small distributions around 60° and 300°. The anisotropic character becomes much more significant with the increase of the electron impact energy, namely, the tetrad petallike pattern appears at 8.2 eV and becomes more distinct at 8.7 eV [see Figs. 2(b) and 2(c)]. As discussed in the following text, the anisotropy of the momentum distribution at these two higher energies can be interpreted with the parity of the Feshbach resonant state $^2\Pi_g$. A quite interesting question arises, namely, what dynamics is controlling the dramatic change of the image patterns from 7.7 to 8.2 eV?

At these three energies, we also find the weak O^- intensities at the center of the images. According to the principle of ion velocity imaging [18,19], the weak intensities at the central slice image imply an ion kinetic energy of near 0 eV. Besides the weak intensities with the low kinetic energy, the O^- anion distributions in a broader energy range obtained by this work and by the others [9,13,20] are plotted in Fig. 3 for comparison. A slice image at 8.1 eV was recorded in a recent parallel study [20], and those experimental data are reproduced with empty circles for comparison in Fig. 3. The present values are normalized with the O^- intensities at a kinetic energy near 0 eV. Except for Dressler and Allan's work [13], both the present work and that of others [9,20] confirm the existence of O^- ions having low kinetic energies. These low-energy O^- anions may be produced simultaneously with the high-vibration-excited CO ($v = 9$–13) [9,20] in the DEA.

In a parallel study by Slaughter *et al.* [20], the slice image at 8.1 eV is extremely similar to the present one recorded at 7.7 eV [Fig. 2(a)]. Such energetic difference may be due to the calibrations for the electron incident energy by the different groups. The uncertainty of the incident energy in the present experiment was estimated to be ± 0.3 eV by the calibration of the standard ionization thresholds of some atoms and molecules.

Before revealing the physics underneath the image pattern evolutions observed in Fig. 2, we should recall the basic theories of the angular DCS of anion produced in the DEA process. On the basis of the formulation by O'Malley and Taylor [21], the angular distribution of the anionic fragment for a diatomic molecule can be determined as

$$\sigma_{\mathrm{DEA}}(k,\theta,\phi) \propto \sum_{|\mu|} \left| \sum_{l=|\mu|}^{\alpha} a_{l\mu} Y_{l\mu}(\theta,\phi), \right|^2 \qquad (1)$$

where k is the incident electron momentum, $a_{l\mu}(k)$ is the energy-dependent expansion coefficient, and $Y_{l\mu}$ is the

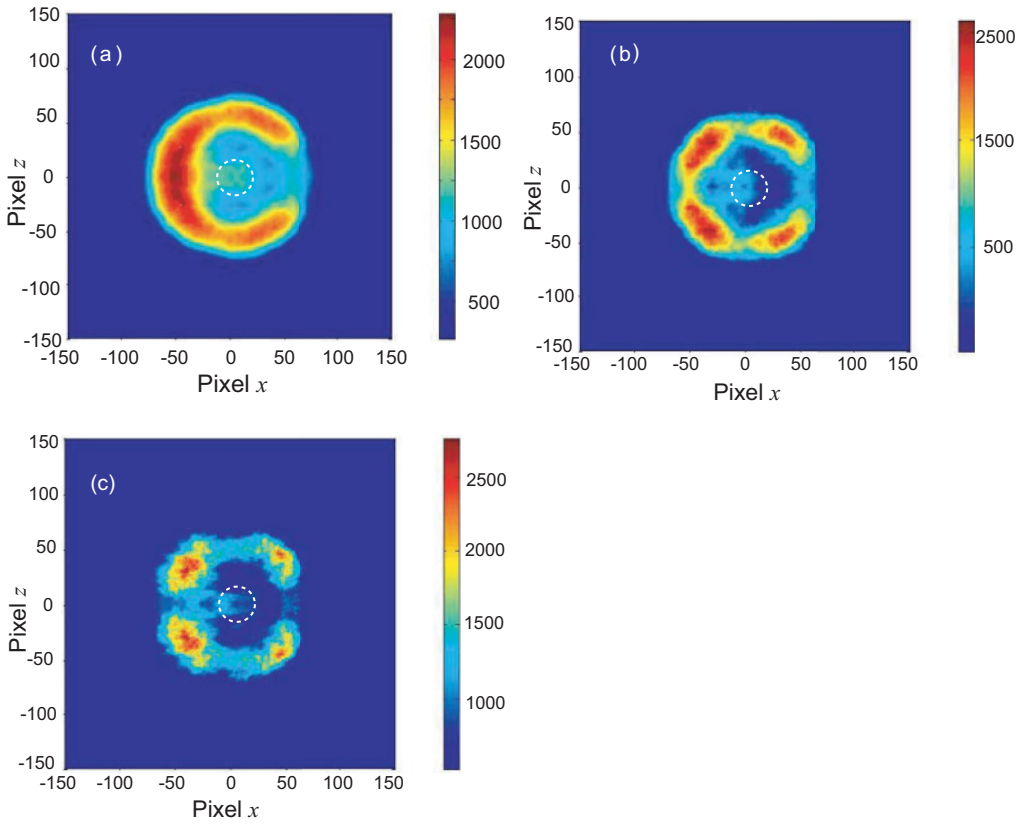

FIG. 2. (Color online) The sliced images of O^- recorded at incident energies of 7.7 eV (a), 8.2 eV (b), and 8.7 eV (c). The small circles (broken white lines) represent the low-kinetic-energy ions. The electron incident direction is from left to right.

spherical harmonics. Here $|\mu| = |\Lambda_f - \Lambda_i|$, representing the difference in the projection of the angular momentum along the internuclear axis for the neutral molecule and the TNI; l is the angular momentum of the incoming electron with values $l \geqslant |\mu|$. This formula was derived from the adiabatic approximation [21] and assuming that the states of the TNI do not interfere. These states are purely additive in a certain proportion for their contributions to σ_{DEA}.

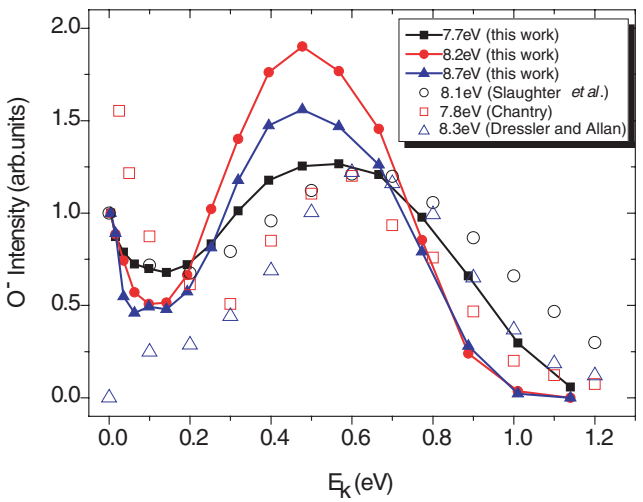

FIG. 3. (Color online) Measured O^- kinetic energy distributions for the different incident electron energies: The data at 7.7, 8.2, and 8.7 eV were obtained in this work; the previous experimental data of Chantry [9], Dressler and Allan [13], and Slaughter *et al.* [20] are adopted for comparison.

As discussed previously for the $^2\Pi_u$ shape resonant state, two components $^2A_1$ and $^2B_1$ as the asymptotic states, are formed due to the RT effect, but they are metastable states and far from the Franck-Condon region of vertical attachment [6]. The complex PES around the $^2\Pi_g$ Feshbach resonant state will also undergo splitting when the vibrational bending mode υ_2 is excited in the electron attachment. As the result of the RT effect, the two asymptotic states split from $^2\Pi_g$ should be also far from the Franck-Condon region. Therefore, the near-zone (not asymptotic) properties of the $^2\Pi_g$ state should be in charge of the anion momentum distributions if the DEA path is across this near zone. Since the dissociation behavior $CO_2^- \rightarrow CO + O^-$ can be approximately treated as the dissociation of a diatomic molecule, the theory of O'Malley and Taylor [21] is applicable in the present case on the basis of the following considerations.

However, only considering the Π parity of the $^2\Pi_g$ state in Eq. (1), we failed in interpreting the image pattern of the O^- momentum distributions in Fig. 2(a). The state splitting in the near zone of $^2\Pi_g$ resonance should be considered. In the $^2\Pi_g$ state-splitting process due to the RT effect, neither Λ nor l is good quantum number, but the vibronic angular momentum K about the axis is a good quantum number, $K = |\pm\Lambda + l|$. The vibronic symmetry can be given by multiplying

the electronic and vibrational symmetries. Therefore, at the Π_g resonant state, when one quantum of the bending vibration mode υ_2 is excited,

$$\Gamma(\psi_{ev}) = \Pi_g \times \Pi_g = \Sigma_u^+ + \Sigma_u^- + \Delta_u, \quad (2)$$

where $\Gamma(\psi_{ev})$ is the irreducible representation of the electron-vibrational wave function ψ_{ev} (beyond the Born-Oppenheimer approximation); Σ and Δ parities correspond to $K = 0$ and $K = 2$, respectively. Since the excitation of the vibrational bending mode υ_2 participates in the DEA, the axial-recoil approximation [22] is broken down. However, the split states in the $^2\Pi_g$ state near zone can be approximated to be the DEA predissociation states, where the geometrical change from the linear to the bending conformer is very small. The axial-recoil approximation [22] might be still valid, while the Σ and Δ parities rather than $^2\Pi_g$ control the O^- momentum distributions. Therefore, the angular distribution of O^- momentum at 7.7 eV shown in Fig. 2(a) can be approximately described with O'Malley and Taylor's theory [21]. Due to the RT effect-induced splitting of the complex PES at the $^2\Pi_g$ Feshbach state and according to Eq. (1), the vibronic angular quanta K of Σ and Δ lead to $\mu = 0$ and 2, respectively. If these two components contribute to σ_{DEA}, we can obtain the best fit by using the summation form $|aY_{00} + be^{i\delta_1}Y_{10} + ce^{i\delta_2}Y_{20}|^2 + |dY_{22}|^2$, which is shown with the black thick line in Fig. 4(a). Here Y_{00}, Y_{10}, and Y_{20} jointly correspond to the Σ parity, while Y_{22} corresponds to the Δ parity. Here δ_i $(i = 1, 2)$ is the relative phase lag for each partial wave of the incident electron, due to the different influences by the target molecular potential for the incident electrons having the different angular momentums l. The fitted $a : b : c : d = 1.0 : 15.2 : 11.6 : 19.1$, and the relative phase lags with respect to that of the s $(l = 0)$ wave are $\delta_1 = 1.344$ rad (p wave, $l = 1$) and $\delta_2 = 1.133$ rad (d wave, $l = 2$). This best fit implies that the $p\Sigma$, $d\Sigma$, and $d\Delta$ scattering amplitudes are predominant at 7.7 eV. The reliability of the above fitting can be further proved by the trial fitting with the form of $|aY_{00} + be^{i\delta_1}Y_{10} + ce^{i\delta_2}Y_{20}|^2$ [only considering Σ parity, which is shown with the red thick line in Fig. 4(a)], indicating the serious deviations from the experimental data.

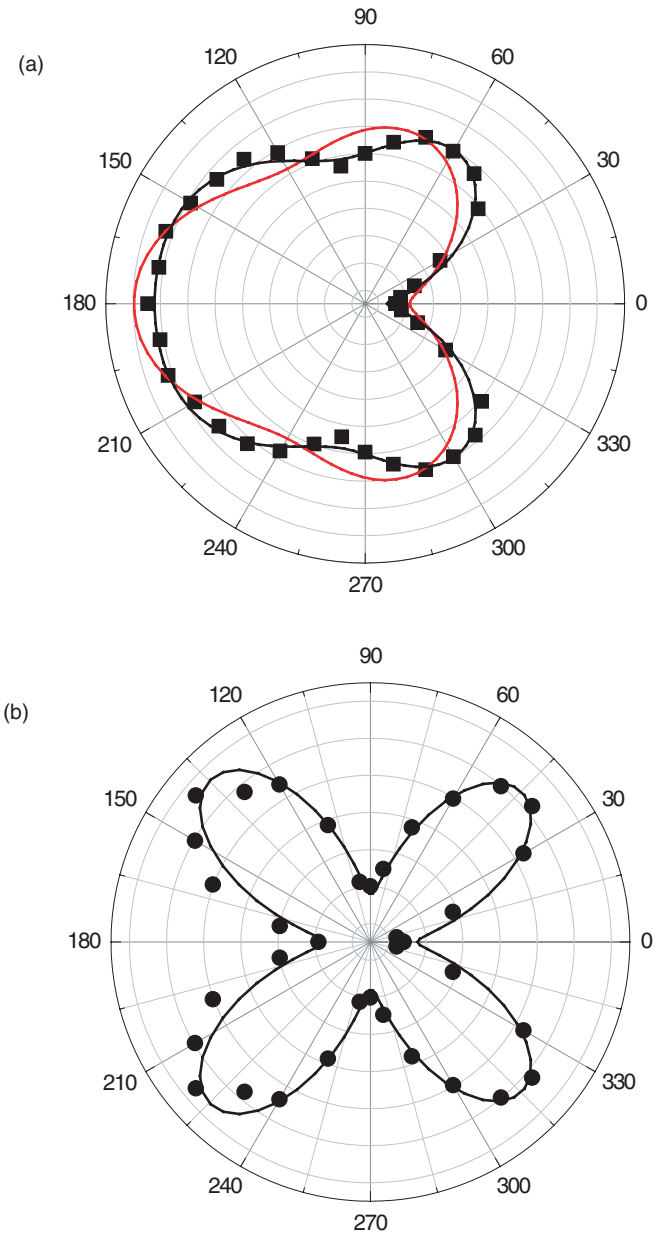

FIG. 4. (Color online) (a) Angular momentum distributions of O^- at an incident energy of 7.7 eV: the best fitting with the form $|aY_{00} + be^{i\delta_1}Y_{10} + ce^{i\delta_2}Y_{20}|^2 + |dY_{22}|^2$ (the black thick line) and the trial fitting with the form $|aY_{00} + be^{i\delta_1}Y_{10} + ce^{i\delta_2}Y_{20}|^2$ [the red (dark gray) thick line]. (b) Angular momentum distributions of O^- at an incident energy of 8.7 eV: the best fitting with the form $|a'Y_{11} + b'e^{i\delta'}Y_{21}|^2$ (the black thick line). The experimental data labeled with squares (a) and circles (b) represent the O^- anions within the kinetic energy range of 0.35–0.65 eV.

In contrast to the angular distribution of O^- momentums at 7.7 eV, the significant anisotropy observed at 8.7 eV cannot be simulated with either of above two forms. As shown in Fig. 4(b), the angular momentum distribution of O^- at 8.7 eV can be well fitted using the form $|a'Y_{11} + b'e^{i\delta'}Y_{21}|^2$, which is simply related to the resonant state $^2\Pi_g$ (using $\Lambda_f = 1$ and $\mu = 1$). The fitted values $\delta' = 1.947$; a' and b' have a ratio of 1:10.9. These fitted parameters indicate that a $d\Pi$ scattering amplitude is predominant at 8.7 eV. In a similar scenario, the angular distribution of O^- momentum at 8.2 eV [see Fig. 2(b)] basically arises from the $d\Pi$ scatterings, although it slightly appears to have forward-backward asymmetry. The predominant scattering amplitude at 8.2 and 8.7 eV is $d\Pi$ while the $p\Sigma$, $d\Sigma$, and $d\Delta$ scattering amplitudes play a role at 7.7 eV, implying the distinctly different DEA mechanisms at these energies.

According to the theoretical potential energy curve (the cyan solid curve in Fig. 3(a) of Ref. [20]), the dissociation to along the C-O single bond is preferred both in energy and in dynamics when the TNI CO_2^- is formed around 8.5 eV. If this dissociation pathway is predominant, the Π parity of $^2\Pi_g$ should be responsible for the angular distribution of O^- momentums, which is in good agreement with the present observation that the $d\Pi$ scattering amplitude is predominant at 8.2 and 8.7 eV. Therefore, the direct dissociation processes by stretching the C-O single bond should be predominant at these two higher energies.

IV. CONCLUSION

In summary, the stereodynamics of DEA to CO_2 is investigated by the O^- anion velocity imaging experiments. Two big bands in the O^- production efficiency spectrum are observed at 4.4 and 8.2 eV, and they are attributed to the $^2\Pi_u$ shape resonant state and the $^2\Pi_g$ Feshbach resonant state of $CO_2{}^-$, respectively. On the low-energy (at 7.7 eV) shoulder of the second band around 8.2 eV, the state splitting in the near-zone $^2\Pi_g$ resonance due to the RT effect leads to the significant backward-scattering pattern of O^- momentum distributions, in which the vibration bending mode υ_2 is excited and the axial-recoil approximation is supposed to be still valid. However, at the higher energies (8.2 and 8.7 eV) of this band, the vertical attachment leads to the impulsive dissociation along the C-O single bond for $CO_2{}^-$ in the $^2\Pi_g$ resonant state.

ACKNOWLEDGMENTS

This work is partially supported by MOST (Grant No. 2011CB921401) and FRFCU (Grant No. WK2340000012).

[1] G. Herzberg and E. Teller, Z. Phys. Chem. Abt. B **21**, 410 (1933); R. Renner, Z. Phys. **92**, 172 (1934).
[2] J. M. Brown and F. Jørgensen, in *Advances in Chemical Physics*, edited by I. Prigione and S. A. Rice (Academic Press, New York, 1983), Vol. 52, p. 127.
[3] E. Illenberger and J. Momigny, in *Gaseous Molecular Ions*, edited by H. Baumgärtel, E. U. Franck, and W. Grünbein (Springer, New York, 1992).
[4] C. J. Noble, K. Higgins, G. Wöste, P. Duddy, P. G. Burke, P. J. O. Teubner, A. G. Middleton, and M. J. Brunger, Phys. Rev. Lett. **76**, 3534 (1996).
[5] M. Allan, Phys. Rev. Lett. **87**, 033201 (2001).
[6] L. A. Morgan, Phys. Rev. Lett. **80**, 1873 (1998); C. W. McCurdy, W. A. Isaacs, H.-D. Meyer, and T. N. Rescigno, Phys. Rev. A **67**, 042708 (2003).
[7] G. J. Schulz, Phys. Rev. **128**, 178 (1962).
[8] D. Rapp and D. D. Briglia, J. Chem. Phys. **43**, 1480 (1965).
[9] P. J. Chantry, J. Chem. Phys. **57**, 3180 (1972).
[10] R. Abouaf, R. Paineau, and F. Fiquet-Fayard, J. Phys. B: At. Mol. Phys. **9**, 303 (1976).
[11] M. Tronc, L. Malegat, and R. Azria, Chem. Phys. Lett. **92**, 551 (1982).
[12] S. K. Srivastava and O. J. Orient, Phys. Rev. A **27**, 1209 (1983).
[13] R. Dressler and M. Allan, Chem. Phys. **92**, 449 (1985).
[14] C. R. Claydon, G. A. Segal, and H. S. Taylor, J. Chem. Phys. **52**, 3387 (1970).
[15] W. B. England, B. J. Rosenberg, P. J. Fortune, and A. C. Wahl, J. Chem. Phys. **65**, 684 (1976).
[16] M. A. Huels, L. Parenteau, P. Cloutier, and L. Sanche, J. Chem. Phys. **103**, 6775 (1995).
[17] S. Goursaud, M. Sizun, and F. Fiquet-Fayard, J. Chem. Phys. **68**, 4310 (1978); M. Sizun and S. Goursaud, *ibid*. **71**, 4042 (1979).
[18] B. Wu, L. Xia, H.-K. Li, X.-J. Zeng, and S. X. Tian, Rev. Sci. Instrum. **83**, 013108 (2012).
[19] C. R. Gebhardt, T. P. Rakitzis, P. C. Samartzis, V. Ladopoulos, and T. N. Kitsopoulos, Rev. Sci. Instrum. **72**, 3848 (2001).
[20] D. S. Slaughter, T. N. Rescigno, D. J. Haxton, A. E. Orel, C. W. McCurdy, and A. Belkacem, J. Phys. B **44**, 205203 (2011).
[21] T. F. O'Malley and H. S. Taylor, Phys. Rev. **176**, 207 (1968).
[22] L. D. A. Siebbeles, M. Glass-Maujean, O. S. Vasyutinskii, J. A. Beswick, and O. Roncero, J. Chem. Phys. **100**, 3610 (1994).